Research of Pattern Formation, edited by R. Takaki, pp. 217–238.

Diffusion-Limited Aggregation and Crystal Growth

Shonosuke OHTA

Physics Department, College of General Education, Kyushu University, Ropponmatsu, Fukuoka 810, Japan

Abstract. Dendritic growth features of the aggregation including surface diffusion processes on two-dimensional square lattice are studied by the Monte Carlo simulation in Laplace field. Preferred direction of the pattern growing with thick branches transfers its anisotropy from <10> direction to <11> one depending on the hopping parameter of surface diffusion which is represented by the ratio of transition probability for the next nearest neighbor surface site to that for the nearest neighbor surface site. Ramifyng structures change from the sidebranching type growing with stable tips to the tip-splitting type with decreasing of anisotropy strength. Self-similar diffusion-limited aggregation (DLA) with a growth mechanism of random tip-splitting type appears in the anisotropy crossover domain under the adequate noise. Another type of DLA, dense-radial-like and crystal-like patterns are also investigated from above viewpoints.

1. Introduction

Much attention has been paid to the dendritic crystallization in the diffusion fields as a problem of interfacial instability and also as a problem of pattern formation in nonlinear and nonequilibrium systems (Ivantsov, 1947; Mullins and Sekerka, 1964; Langer and Muller-Krumbhaar, 1978; Huang and Glicksmann, 1981; Brower *et al.*, 1983; Kessler *et al.*, 1985; Dougherty *et al.*, 1987; Bechhoefer and Libchaber, 1987; See, e.g. Pelcé, 1988).

According to the nonequilibrium condition, various kinds of dendrite have been observed in the supersaturated ammonium chloride (NH_4Cl) solution (Chan *et al.*, 1976; Honjo *et al.*, 1985). A tip-stable type of the <100> dendritic crystal has

been observed in a moderate supersaturation regime of solution. The shape of the tip interface is stable parabola. The rear interface becomes unstable and then side branches are formed. Growth mechanism of the dendrite has been theoretically investigated as the problem of interfacial instability in a non-linear system with the boundary condition of anisotropy or surface tension (Langer, 1980, 1989). Pieters and Langer (1986) have indicated from a boundary-layer model that the successive side branches in the tip-stable dendrite are generated by selective amplification of noise near the tip.

For a very low supersaturated solution a tip-oscillating type of <100> dendrite is obtained. The tip velocity and the tip curvature oscillate in time and the sidebranching mechanism is strongly related to this oscillation. In the much higher supersaturation regime where the most preferred orientation changes from the <100> direction to the <110> direction, NH_4Cl dendritic crystals various kinds of tip-splitting type are observed.

Irregular fractal-like crystal growth from the aqueous solution of NH_4Cl has been detected by the experiment of diffusion controlled crystallization in the Hele Shaw-like cell, one of the glass-plate surfaces of which is roughened to weaken the degree of the crystal-growth anisotropy (Honjo *et al.*, 1986). Its fractal dimension obtained from the radius-of-gyration exponent is 1.671 ± 0.002 and is in very good agreement with the theoretical prediction (Muthukumar, 1983; Tokuyama and Kawasaki, 1984; Honda *et al.*, 1986) for the diffusion-limited aggregation (DLA) model (Witten and Sander, 1981; See, e.g. Family and Landau, 1984; Stanly and Ostrowsky, 1985; Pietronero and Tosatti, 1986; Vicsek, 1989). Moreover, the generalized dimensions and the f-α spectrum for this fractal-like crystal (Ohta and Honjo, 1988) based on the growth-probability-distribution analysis (Halsey *et al.*, 1986; Vicsek, 1989) are in good agreement with the results for the off-lattice DLA simulation and theory (Hayakawa *et al.*, 1987; Matsushita *et al.*, 1987). The relation between regular dendritic crystal and random DLA-like one is discussed by the crystal growth from melting succinonitrile (Honjo *et al.*, 1987). Various growing modes such as asymmetric tip-splitting, symmetric tip-splitting and tip-oscillating growths are obtained in the supercooling-anisotropy phase space.

These experiments of crystal growth indicate that the boundary conditions arising from the anisotropy and noise are essential for the dendritic pattern formation in the diffusion field. In fact, such boundary conditions have been clarified in the experiments of the electrodeposition (Sawada *et al.*, 1986; Grier *et al.*, 1986) and the anisotropy imposed viscous fingering (Ben-Jacob *et al.*, 1985).

On the other hand, experimentally observed DLA patterns by the electrodeposition (Matsushita *et al.*, 1984), dielectric breakdown (Niemeyer *et al.*, 1984), hydrodynamic viscous fingering (Daccord *et al.*, 1986), monomolecular layer (Miller *et al.*, 1986) and dendritic crystal growth (Honjo *et al.*, 1986) construct homogeneous and self-similar structures. Ball and Brady (1985a) and Meakin *et al.* (1987) have found the inhomogeneity of Witten-Sander DLA model growing in the <10> direction from the superposition of many simulated patterns and from the large

scale simulation, respectively. Therefore, it is attractive problem what growth mechanism of the unscreened tips can control whether a pattern grows homogeneously or not.

Various kinds of the aggregation model have been performed to search for the interrelation between DLA and real crystal growth by the introduction of surface tension effect (Vicsek, 1984, 1985; Tao *et al.*, 1988), Monte Carlo averaging (Tang, 1985; Kertész and Vicsek, 1986; Eckmann *et al.*, 1989, 1990), coase-grained lattice (Matsushita and Kondo, 1986), noise parameter (Nittmann and Stanley, 1986) and surface kinetic process (Xiao *et al.*, 1988).

In this paper, we insert a surface diffusion process by means of the random walk of Brownian particle along the pattern surface into the Witten-Sander DLA model on a two-dimensional square lattice. From the Monte Carlo simulation of this model, we investigate the growth features of the dendritic and DLA patterns.

2. Solidification of Surface Diffusion Particles

Surface diffusion particle which occupies a metastable state among the surface energy levels transits to a surface state of another surface site due to the thermal energy. There are two well known processes on the solidification of such particles in the field of crystal growth. The one is the stabilization at the kink point or step site where the surface potential is low. The other is the two-dimensional nucleation arising from the increasing concentration of surface diffusion particles on the principal surface without any kinks or steps. In order to take into account of the latter process, we assume a nucleus composed of m particles, and assume the surface random walk of τ steps after the sticking of Brownian particle until create a nucleus. Here, the surface is defined as the site that something of its nearest neighbor (NN) sites is occupied by the pattern.

While for the former process, surface particle arrived in a kink site has diffusion stopped even if its steps of random walk are less than τ. The kink site is defined as where the adjacent two NN sites as well as a next nearest neighbor (NNN) site between them are occupied by the pattern. In the kink site, we also assume that the pattern grows when the count of arrived particles reaches m, which corresponds to the length of a step in real step growth of the crystal. This value m has been called a noise parameter in the simulation of Nittmann and Stanley (1986) without any surface diffusion process.

Schematic drawing of the Monte Carlo simulation is shown in Fig. 1, where b is a Brownian particle in the Laplace field and d is a surface diffusion particle. Solidification of the surface particle k at the kink site is the step growth type, and that of the surface particle n at the principal surface such as AB plane is the two-dimensional nucleation type.

For the kinetics of surface diffusion particles, we further introduce a hopping parameter which is defined by the ratio of the transition probability for the NNN site to that for the NN site. Assuming the potential barriers of Δ_1 and Δ_2 that surface

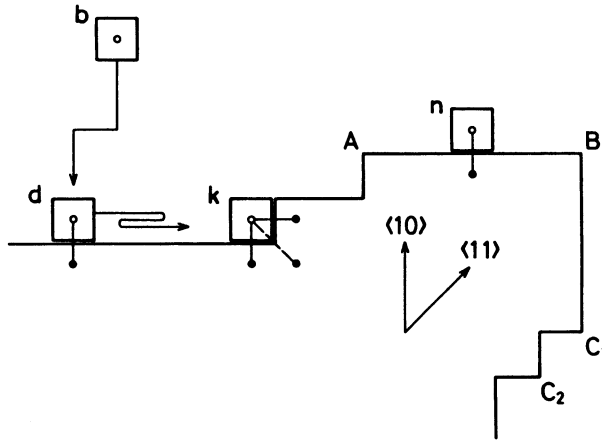

Fig. 1. Schematic drawing of the Monte Carlo simulation on two-dimensional square lattice. Open and closed circles show Brownian and cluster particles, and solid and dotted lines represent the bondings of nearest and next nearest neighbor sites, respectively. And figure shows Brownian particle in Laplace field by *b*, diffusion particle on the pattern surface by *d*, crystallization of surface particle at kink point by *k* and surface nucleation on a plane surface by *n*.

particles undergo at the transit to NN and NNN sites, respectively, hopping parameter is described as $\gamma = \exp\{(\Delta_1 - \Delta_2)/kT\}$. A transfer surface site is chosen from all of NN and NNN surface sites around the present position by the Monte Carlo method with the selection weight of one for NN site and that of γ for NNN site. After the trial of τ steps or arriving at the kink point, we have the memory of located surface site counted up. In a special case for the sum total of selection probability to be zero under $\gamma = 0$, we have diffusion particle stopped at the present surface site. In case of small γ surface diffusion is limited within a plane surface, but in case of large γ surface particle enable to transfer to a different plane through the hopping process to the NNN site. Following simulations begin from a seed particle putted on the center of $x = y = 0$ as same as the ordinary DLA simulations. However, maximum flight length l_b of Brownian particle in the field is chosen by $l_b \leq 5 + \sqrt{\tau}$ lattice units instead of $l_b = 5$ in Witten-Sander DLA simulated by Meakin (1986a), and the radius where Brownian particles are killed is selected by $r + sl_b$ instead of $3r$ of ordinary simulations, where r is the maximum radius of the pattern and s is the fixed number of $s \geq 15$. These selections give the consistent fractal dimensions with those obtained previously as indicated in the Witten-Sander DLA and off-lattice DLA simulations of below sections. By means of those simulations, computing time can be reduced. Almost all simulations are performed up to the radius of $r =$ 600 lattice units.

3. Dendritic Pattern Formation with Different Anisotropies

Typical examples of the simulated patterns obtained from fixed $m = 1$ and $r = 600$ are shown in Fig. 2. Even in the case of $\tau = 1$, anisotropic pattern grows in the <10> direction at $\gamma = 0$ of Fig. 2(a), and grows in the <11> direction at $\gamma = 1$ of Fig. 2(c) by means of the mechanism of kink growth. Really, in a *kink-off* simulation which assumes the lack of kink effect, homogeneous DLA-like pattern grows as shown in Fig. 2(e), where every surface particle has carried out the surface random walk of $\tau = 1$ step. These results indicate that the solidification at the kink point plays an important role for the anisotropic pattern formation.

The strength of pattern anisotropy increases with increasing of τ as is seen in

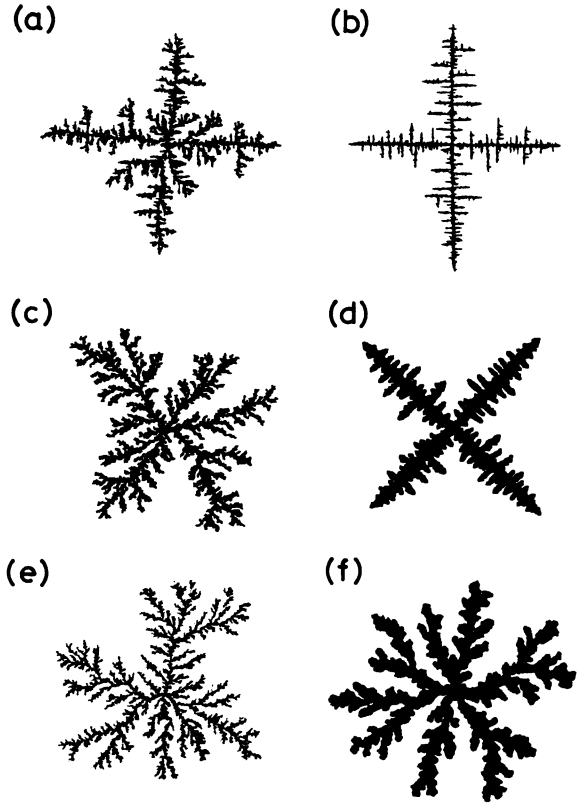

Fig. 2. Typical examples of the simulated patterns with the radius of $r = 600$ lattice units obtained from fixed $m = 1$. *Kink-on* patterns, (a) $\gamma = 0$, $\tau = 1$, N = 65,000, (b) $\gamma = 0$, $\tau = 100$, N = 61,000, (c) $\gamma = 1$, $\tau = 1$, N = 110,000, (d) $\gamma = 1$, $\tau = 100$, N = 192,000, yield anisotropy. While the anisotropy of *kink-off* patterns, (e) $\gamma = 1$, $\tau = 1$, N = 114,000, (f) $\gamma = 1$, $\tau = 100$, N = 298,000, are invisibly small.

Figs. 2(b) and 2(d) of *kink-on* simulations with $\tau = 100$. However, in case of *kink-off* simulation with $\tau = 100$ its anisotropy is invisibly small as shown in Fig. 2(f), whose fractal dimension is $d_f = 1.716 \pm 0.010$ for the average of 90 samples of the particle numbers N = 215,000. Such a result is in good agreement with $d_f = 1.715$ of off-lattice DLA simulation by Meakin and Sander (1985). Randomly ramifying structures are also different from the sidebranching type in the anisotropic patterns of Figs. 2(b) and 2(d).

For this *kink-off* pattern, we can estimate the average thickness w of branches from the relation of $N = {}_{w}r^{d_f}$. The result shows $w \sim \tau^{1/4}$ on the dependence of τ up to 200 steps. Since the surface diffusion length is described as $l_d = \sqrt{\tau}$ for the random walk of τ steps, such a dependence $w \sim l_d^{1/2}$ indicates that the surface structures of the *kink-off* patterns are recognized as the two-dimensionally rough surface such as the Peano curve (Mandelbrot, 1977). While, the thickness of branches for the <11> dendritic pattern in $\gamma = 1$ like as Fig. 2(d) is proportional to l_d by means of direct measurements of w. In such a pattern, tip front of main branches has faceted surfaces at its both sides as referenced in AB and BC_1 planes of Fig. 1. The length of faceted surface which is calculated as the mean length of BC_1 (first step) and BC_2 (second step) for the <10> direction excellently agrees with l_d. On the other hand, for the <10> dendritic patterns of $\gamma = 0$ characteristic lengths such as the thickness of main branches and the distance between successive side branches are not so clear on the dependence of τ. It seems that the effective surface diffusion length becomes less than $\sqrt{\tau}$ because the surface diffusion processes are limited within a plane surface. Therefore, the thickness of Fig. 2(b) is very thin comparing with that of Fig. 2(d). In case of $\tau \geq 10^5$ at $\gamma = 0$, <10> needlic pattern appears without any sidebranchings up to the pattern size of $r = 600$.

4. Anisotropy of Dendritic Pattern

Varying features of the anisotropic pattern obtained from the *kink-on* simulation of fixed $m = 5$ and $\tau = 10$ are shown in Fig. 3. These results indicate that γ is an effective control parameter for the pattern anisotropy. In case of small γ the tip front has rough surface composed of kinks and the surface diffusion process is limited within a plane surface. Therefore, solidification of the particles adsorbed in the tip front derives the pattern growth towards the <10> direction. While in case of large γ, such adsorbed particles can penetrate into the screened surface near the tip due to the diffusion process transfer to the NNN site, and then such a tip as facets form in its both sides develops through the solidification at kink sites. As a result of the nucleation and kink growth on both faceted surfaces, the tip grows in the <11> direction. Hence, we can understand that the dominant process of the tip growth is frontal type under the condition of $\gamma < \gamma_c$ and lateral type under that of $\gamma > \gamma_c$, where γ_c is the hopping parameter at the crossover point between <10> and <11> anisotropies.

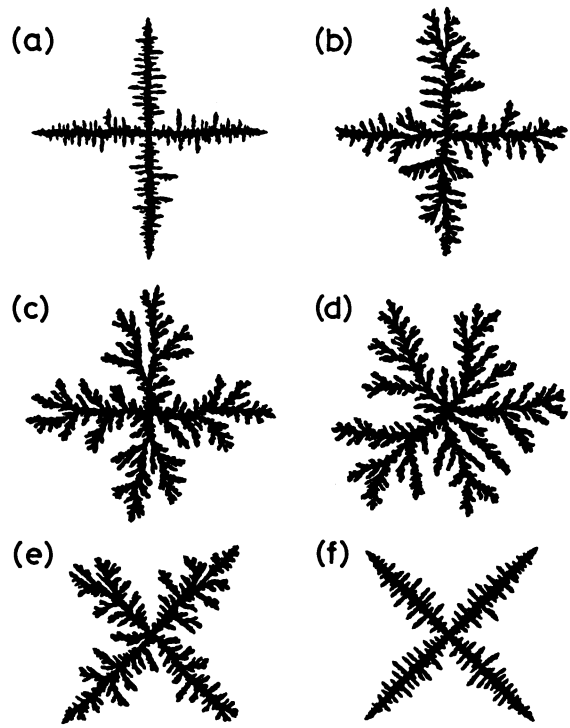

Fig. 3. Examples on the dependence of hopping parameter for fixed $m = 5$, $\tau = 10$ and $r = 600$. The hopping parameters are γ = (a) 0.05, (b) 0.175, (c) 0.2, (d) 0.23, (e) 0.3 and (f) 0.6. The particle numbers constituting the patterns are N = (a) 124,000, (b) 211,000, (c) 251,000, (d) 293,000, (e) 200,000 and (f) 147,000. Averaged pattern anisotropies for many samples are α = (a) 0.71, (b) 0.51, (c) 0.37, (d) 0.01, (e) –0.51 and (f) –0.70.

In order to obtain γ_c we measure the anisotropy of patterns as follows: A pattern is divided into four parts by the two lines of $x = \pm y$, and then the radii of gyration $k_{10\parallel}$ and $k_{10\perp}$ along the <10> direction are obtained as the average values of four parts, where $k_{10\parallel}$ and $k_{10\perp}$ stand for the characteristic lengths of main and side branches in the <10> dendritic pattern, respectively. At the same time, from the patterns of four parts divided by the two lines of $x = 0$ and $y = 0$, we obtain the radii of gyration $k_{11\parallel}$ and $k_{11\perp}$ along the <11> direction characterizing the lengths of main and side branches of the <11> dendritic pattern. Finally, pattern anisotropy is calculated from a definition of $\alpha \equiv (k_{11\perp} - k_{10\perp})/(k_{11\perp} + k_{10\perp})$ represented by the characteristic lengths of sidebranches. The features of α depending on γ are shown in Fig. 4, where we used the average of 20 samples (50 samples of N = 215,000 only in case of $\gamma = 0.23$). The <10> and <11> dendritic patterns are described as $0 < \alpha < 1$ and $-1 < \alpha < 0$, respectively. This measure shows $\alpha = 0$ for disk, $\alpha = -0.172$

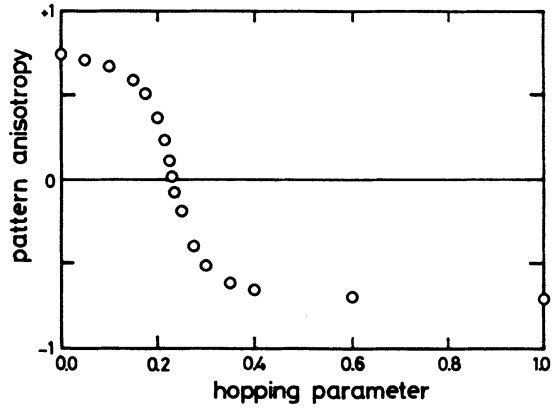

Fig. 4. Varying features of the pattern anisotropy α for fixed $m = 5$ and $\tau = 10$ as a function of the hopping parameter γ. The crossover point of $\alpha = 0$ gives $\gamma_c = 0.233 \pm 0.005$.

for square, $\alpha = 0.172$ for diamond, $\alpha = 1$ for + pattern and $\alpha = -1$ for × pattern. From these results for $m = 5$ and $\tau = 10$ we get $\gamma_c = 0.233 \pm 0.005$ as the value of γ at $\alpha = 0$. Therefore, Fig. 3(d) indicates a crossover pattern between the two anisotropies of <10> and <11> dendritic growths.

5. Morphological Phase Diagram of Dendritic Pattern

Crossover points for $m = 1$, 5 and 100 obtained from above method are plotted in Fig. 5 as a morpological phase diagram of hopping parameter γ versus surface diffusion steps τ. The <10> dendritic pattern grows in the range of small values of γ and τ, on the other hand the <11> dendritic pattern appears in the range of large values of γ and τ. The crossover line of $m = 1$(●) between <10> and <11> anisotropy domains satisfies $\gamma_c\sqrt{\tau} \cong 1.0$, i.e., $\gamma_c \cong 1/l_d$ for $\tau >> 1$. Such a relation implies that the crossover condition is determined by the balance between the probability $1/l_d$ situated in the edge of plane surface with the length l_d and the relative transfer probability γ to translate into another plane by the NNN site hopping.

While, the crossover lines for $m = 5$(×) and 100(○) are situated below that for $m = 1$, i.e., $\gamma_c \cong \tau^{-0.62}$ for $m = 5$ and $\gamma_c \cong \tau^{-0.79}$ for $m = 100$ in $\tau >> 1$. Such phenomena can be understood from the two averaging effects based on the increment of m and the surface diffusion process, and also can be understood from the difference of surface structures between {10} and {11} planes. The increase of m takes effect on the smoothing of the diffusion field due to the averaging process of the randomness, and this effect equally acts on the {10} and {11} planes. While the surface diffusion process takes effect on the smoothing of the surface concentration and that of the surface nucleation growth. This effect acts only on the {10} plane, but there is no

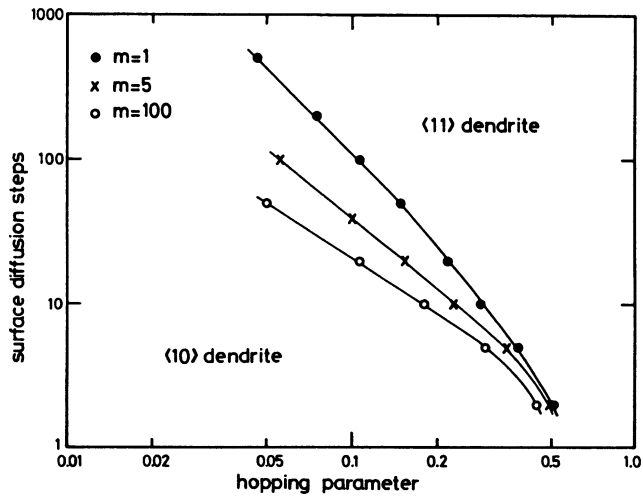

Fig. 5. Morphology diagram of dendritic pattern on the phase space of hopping parameter γ vs. surface diffusion steps τ. Plots indicate the crossover points between <10> and <11> dendritic pattern for fixed m = 1(●), 5(×) and 100(○).

effect on the {11} plane covered with kinks because surface diffusion is forbidden. Such smoothing effects on the {10} plane enhance with increase of m.

Let us consider a {10} surface without kinks such as AB plane in Fig. 1. In case of $m = 1$, nucleation growth on this plane occurs in an arbitrary site according to the random number used in the Monte Carlo method. On the other hand, in case of large m probability of the nucleation growth at the center of this plane, increases by the smoothing effects mentioned above. New {10} plane is formed both sides from this nucleus by the step growth. Therefore, the increment of m constructs a smoother surface in the {10} plane than in the {11} plane under the conditions of fixed γ and τ. Such considerations indicate that the surface (line) tension increases in the <10> orientation. As a result of this effect, pattern grows in the <11> direction with weak surface tension. In fact, the increment of m derives the pattern growth with thick branches and with <11> anisotropy.

Various patterns for $m = 100$ with the smoothing effect and with the anisotropy of surface tension are shown in Fig. 6. The pattern of Fig. 6(a) with $\alpha = 0.859$ obtained from $\gamma = 0$ and $\tau = 100$ has stable tips in the front of main branches, which is excellently similar to a typical form of real dendritic crystal growth. Front surface of the tips is composed of kinks, and its rear surface becomes unstable. This result interests in connection with the problem of interfacial instability (Pieters and Langer, 1986) for the tip-stable type of real dendritic crystal growth such as NH_4Cl crystal (Honjo *et al.*, 1985). In there conditions, the increment of τ drives a needle-

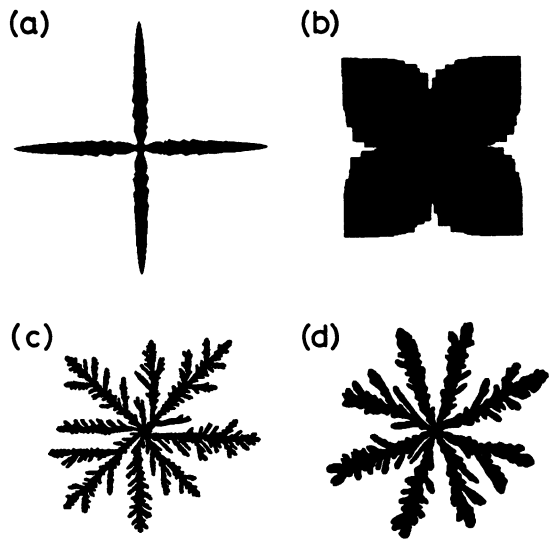

Fig. 6. Typical examples of simulated patterns obtained from fixed m = 100. Simulated conditions are (a) $\gamma = 0$, $\tau = 100$, $r = 400$, N = 52,000, (b) $\gamma = 1$, $\tau = 10^4$, $r = 400$, N = 290,000, (c) $\gamma = 0.46$, $\tau = 2$, $r = 600$, N = 224,000 and (d) $\gamma = 0.18$, $\tau = 10$, $r = 600$, N = 319,000. Growth features are (a) tip-stable dendritic type, (b) hopper type, (c) anisotropy coexistent type and (d) anisotropy intermediate type.

like pattern with smooth rear surface (Langer, 1986; Barbieri *et al.*, 1987; Liu and Goldenfeld, 1988). These results indicate that the increments of m and τ are efficacious against the interfacial instability.

Leading process of the pattern formation in Fig. 6(b) of $\gamma = 1$ and $\tau = 10^4$ is the lateral growth mechanism due to the step and nucleation growth on faceted surfaces. It shows a regular pattern when the length of faceted surfaces are less than l_d, i.e., at $N \leq 4l_d^2 = 40{,}000$, and then it forms a hopper-like pattern with giant steps as seen in Fig. 6(b). According to the conditions of surface diffusion mechanism, present kink-on simulations yield two similar patterns to real crystal growth.

The examples of crossover pattern for $m = 100$ are shown in Figs. 6(c) and 6(d), the morphology of which is quite different from that for $m = 5$ of Fig. 3(d) due to the existence of anisotropical surface tension effects based on the averaging process. The morphology of Fig. 6(c) for $\tau = 2$ indicates an anisotropy coexistent type with mixed <10> and <11> anisotropic branches, where γ takes 0.46. While, that of Fig. 6(d) for $\tau = 10$ and $\gamma = 0.18$ shows an anisotropy intermediate type that the main branches grows with the middle preferred direction between <10> and <11> directions. Such a morphological change occurs at $\tau = 4 \sim 5$, i.e., $l_d \sim 2.1$. These results imply that the surface tension in the middle orientation weakens as $l_d \geq 2.1$, and that the growth mechanism of tips becomes the asymmetric tip-splitting type

as seen in the experiment of diffusion controlled crystallization (Honjo *et al.*, 1987). Thus, the existence of averaging mechanisms produces the anisotropy of surface tension through the surface diffusion processes.

6. Diffusion-Limited Aggregation in *kink-on* Simulation

Characteristic feature of DLA is homogeneous and self-similar structures without any anisotropy. On the pattern formations of the homogeneous DLA as well as the anisotropic dendrite, only a few hottest tips can practically grow outside of the pattern, which mainly determines its framework. Therefore, it is an important problem to understand the pattern formation growing in the diffusion field what growth mechanism of the hottest tips can control whether a pattern grows homogeneously or not.

We introduced a measure of α in order to get the anisotropy of the patterns in previous section. All of crossover patterns in *kink-on* simulation as seen in Figs. 3(d) and 6(c) and 6(d) show $\alpha \sim 0$. However, it is clear that the crossover patterns for $m = 100$ have the inhomogeneity reflected in the coexistent or intermediate states of the anisotropies. Therefore, in order to detect the homogeneity of patterns, we need to use another type of measure. For this purpose, we calculate the two types of fractal dimension based on the different standpoints.

We study the scaling properties of *kink-on* patterns at first by using the finite-size scaling analysis (Meakin and Family, 1986b). Two exponents $\nu_{\|}$(○) and $\nu_{\perp}$(●) obtained from the relations of $k_{\|} \sim N^{\nu_{\|}}$ and $k_{\perp} \sim N^{\nu_{\perp}}$ are shown in Fig. 7(a) as a function of α for fixed $m = 5$ and $\tau = 10$, where the data of $k_{10\|}$ and $k_{10\perp}$ ($k_{11\|}$ and $k_{11\perp}$) are used for the patterns of $\alpha > 0$ ($\alpha < 0$). Therefore, $\nu_{\|}$ and $\nu_{\perp}$ indicate the characteristic exponents of the main and side branches for the dendritic pattern, respectively. Since the crossover pattern of $\alpha \sim 0$ as shown in Fig. 3(d) has $\nu_{\|} \cong \nu_{\perp}$ in Fig. 7(a), we can understand its structure in a self-similar fractal with the same scaling properties for the main and side branches. But the other anisotropic patterns yield self-affine fractals (Mandelbrot, B. B., 1982) with different scaling exponents between main and side branches. The fractal dimension based on this finite-scaling analysis has been derived as $D = 1 + (1 - \nu_{\|})/\nu_{\perp}$, which is a dimension described within the region of the pattern to be able to adapt to the anisotropic patterns. Namely, a main branch of length $k_{\|}$ is composed of lumps of size $k_{\perp}$. Assuming the fractal dimension D within the lump, particle numbers constituting a lump is $k_{\perp}^{D}$, and then particle numbers of the main branch is $k_{\|}/k_{\perp}$ times as much as that. Above equation for D is obtained from the equality in the exponents of $N \sim (k_{\|}/k_{\perp})k_{\perp}^{D}$ by substituting before relations for $k_{\|}$ and $k_{\perp}$. Self-similar pattern of $\nu_{\|} = \nu_{\perp} = \nu$ gives $D = 1/\nu$. The results of D(○) calculated from the exponents of Fig. 7(a) are shown in Fig. 7(b).

While, ordinary fractal dimension d_f is defined by the exponent of the radius of gyration around a vertical axis to the pattern plane, which represents the characteristic behavior of the occupied space by the pattern comparing with the

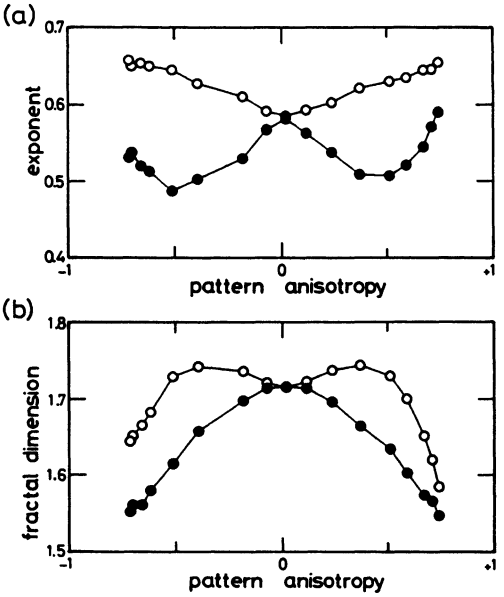

Fig. 7. (a) Characteristic exponents $\nu_{\parallel}$(○) and $\nu_{\perp}$(●), and (b) fractal dimensions D(○) and d_f(●) drawn as a function of pattern anisotropy for the *kink-on* simulations in $m = 5$ and $\tau = 10$.

overall space. Hence, it can be expected that D is always larger than d_f excepting a homogeneously spreaded pattern over the whole space. As shown in Fig. 7(b) d_f(●) gives maximum value at $\alpha \sim 0$, and also extremely agrees with D(○) at $\alpha \sim 0$, where $d_f = 1.716 \pm 0.003$ and $D = 1.715 \pm 0.010$ for $m = 5$, $\tau = 10$, $\gamma = 0.23$ and $N = 215{,}000$.

From the above results, we can conclude that this crossover pattern forms the isotropic, homogeneous and self-similar DLA, because it has $\alpha = 0$, $D = d_f$ and $\nu_{\parallel} = \nu_{\perp}$ within the error, and also because its fractal dimensions $D \cong d_f \sim 1.716$ excellently agree with the result of $d_f = 1.715$ in the off-lattice DLA simulation (Meakin and Sander, 1985). Hereafter, we call it *kink-on* DLA.

On the growth mechanism of hottest tips constructing a homogeneous and self-similar DLA, we can estimate from the various results for the *kink-on* simulations obtained until now. Morphology of ramifying structures changes from the sidebranching type to the tip-splitting type with decreasing of the anisotropy strength as indicated in Fig. 3. Taking care of Figs. 3(b) and 3(e), tip of main branch sometimes symmetrically split into two branches with small unfolding angle such as observed in succinonitrile experiment (Honjo *et al.*, 1987). Reflecting this phenomenon $\nu_{\perp}$ takes minimum value of about 0.5 at $|\alpha| \sim 0.5$ in Fig. 7(a), which means the compact structure of $1/\nu_{\perp} \sim 2.0$ in the direction perpendicular to the tip growth.

Such anomalies imply that the morphorogical change of main branch from tip-stable to tip-splitting modes occurs in the anisotropy strength of $|\alpha| \sim 0.5$.

Next, let us pay attention to the angles of sidebranching and tip-splitting structures. Unfolding angle of tip-splitting increases with decreasing of anisotropy strength $|\alpha|$ as is seen in Fig. 3 according to the order of (b), (c) and (d). On the contrary, sidebranching angle which is initially equal to right angle as shown in Fig. 3(a) decreases with decreasing of $|\alpha|$ in order of figure. We infer from the self-similarity of $\nu_{\parallel} = \nu_{\perp}$ for crossover pattern that two characteristic angles are equalized each other in $|\alpha| = 0$. According to such a conjecture DLA structures are constructed by the random tip-splitting mechanism growing without the classification between main and side branches.

Random tip-splitting mechanism depends on the randomness arising from noise in the field and/or from fluctuation on the pattern surface as mentioned before. Here, we discuss the fractalities for anisotropy coexistent and intermediate types simulated in $m = 100$ with reduced effects of randomness. In the anisotropy coexistent type of $\tau = 2$ as illustrated in Fig. 6(c), average of 25 samples for $\gamma = 0.46$ and $N = 90{,}500$ gives $\alpha = -0.073$, $d_f = 1.660$, $\nu_{\parallel} = 0.622$, $\nu_{\perp} = 0.580$ and $D = 1.652$, and 20 samples for $\gamma = 0.45$ and $N = 90{,}500$ show $\alpha = 0.115$, $d_f = 1.672$, $\nu_{\parallel} = 0.614$, $\nu_{\perp} = 0.563$ and $D = 1.684$. Results indicate almost homogeneous pattern of $d_f \cong D \sim 1.66$, but indicate obviously self-affine pattern with different growth properties between main and side branches, i.e., difference between $\nu_{\parallel}$ and $\nu_{\perp}$ shows about 0.04. As a result of the sidebranching mechanism by fixed angle of 45 degrees, its fractal dimension becomes smaller than that of *kink-on* DLA, and it is preferably in accordance with theoretical dimension $d_f = 5/3$.

While, in the anisotropy, intermediate type of $\tau = 10$, $\gamma = 0.18$ and $N = 304{,}000$ as shown in Fig. 6(d), average of 5 samples shows $\alpha = 0.006$ and $d_f = 1.731$. Such a large fractal dimension seems to be attributed to the surface instability because of the weak surface tension in the intermediate orientation. Present finite-scaling analysis is unavailable for this pattern with different direction. Simulated pattern in $\tau >> 2.1$ gives various kinds of interesting behavior reflecting surface tension and weak anisotropic effects such as viscous fingering phenomena in Hele Shaw cell (Saffman and Taylor, 1958; Paterson, 1985; Ben-Jacob *et al.*, 1985; Daccord *et al.*, 1986; Liang, 1986; Bensimon *et al.*, 1986; Tao *et al.*, 1988; Langer, 1989; See, e.g. Pelcé, 1988).

Subsequently, even in the *kink-on* simulation including the boundary conditions of the surface diffusion process and kink effect producing the pattern anisotropy, homogeneous and self-similar DLA, i.e., *kink-on* DLA brings into existence in the crossover domain between the <10> and <11> anisotropies under the adequate noise to reduce anisotropies by the mechanism of random tip-splitting growth in the hottest tips.

7. Homogeneity in Various Diffusion-Limited Aggregation Model

According to the judgement of homogeneous and self-similar DLA mentioned above, we investigate the homogeneity and self-similarity in various kinds of DLA model, i.e., Witten-Sander DLA on the two-dimensional square lattice, off-lattice DLA on the two-dimensional plane and *kink-off* DLA on the two-dimensional square lattice as shown in Figs. 2(e) and 2(f). The features of anisotropy evolution are drawn in Fig. 8 on the $k_{10\perp}$ versus $k_{11\perp}$ plane, where plots are Witten-Sander DLA ( ), off-lattice DLA(Δ), *kink-off* DLA(+) with $\tau = 10$ and *kink-on* DLA(○) (d), and Figs. 8(a)–(f) (○) correspond to the *kink-on* simulations of Figs. 3(a)–(f). Here, a line of $k_{10\perp} = k_{11\perp}$ shows $\alpha = 0$.

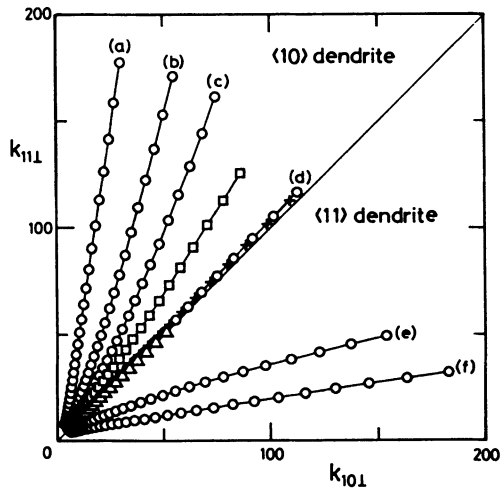

Fig. 8. Evolution of pattern anisotropy drawn on $k_{10\perp}$ vs. $k_{11\perp}$ plane. Here, (a)–(f) correspond to the Fig. 3. (a)–(f) of *kink-on* simulation(○). Other plots are *kink-off* simulation(+) in $\tau = 10$ up to N = 128,000, Witten-Sander DLA model( ) up to N = 54,000 and off-lattice DLA model(Δ) up to N = 27,000.

The Witten-Sander DLA for 200 samples of N = 54,000 yields the pattern anisotropy of $\alpha = 0.190 \pm 0.009$. From the curve fitting by $k_{10\perp} = B_0 N^{A_0}$ and $k_{11\perp} = B_1 N^{A_1}$, we get $A_0 = 0.564$, $B_0 = 0.185$, $A_1 = 0.621$ and $B_1 = 0.145$. It is clear that the Witten-Sander DLA always yields <10> anisotropy from Fig. 8, which increases with increasing of N because of $A_0 < A_1$. Such behaviors are consistent with the results of the large scale simulation by Meakin *et al.* (1987). Substituting $N = 10^6$, 10^8 and 10^{10} into above equations, we get $\alpha = 0.27$, 0.38 and 0.49. Thus,

our estimation says the pattern size of $N > 10^{10}$ needs to get a Witten-Sander DLA pattern with $\alpha = 0.5$. The probability of the arriving particles, from the diffusion field to the surface of a hottest tip, must be greater in the front surface than in the side surface, as indicated in the study of the Monte Carlo averaging (Eckmann *et al.*, 1989, 1990). Accordingly, the Witten-Sander DLA without any surface diffusion processes would be regarded as a type of the frontal growth type rather than the lateral one, and thus the inhomogeneity growing in <10> direction appears. Results of fractality for Witten-Sander DLA are summarized in Table 1.

Table 1. List of the fractal dimensions, characteristic exponents and pattern anisotropy for various kinds of DLA model. Simulated conditions are $m = 5, \tau = 10, \gamma = 0.23$, N = 215,000 and 50 samples for *kink-on* DLA, $m = \gamma = 1, \tau = 10$, N = 128,000 and 300 samples for kink-off DLA, N = 27,000 and 200 samples for off-lattice DLA, and N = 54,000 and 200 samples for Witten-Sander DLA.

Model	d_f	D	$\nu_{\parallel}$	$\nu_{\perp}$	α
kink-on DLA	1.716±0.003	1.715±0.010	0.585±0.002	0.581±0.005	0.013±0.014
kink-off DLA	1.716±0.002	1.712±0.009	0.582±0.002	0.588±0.004	0.016±0.007
off-lattice DLA	1.714±0.002	1.711±0.009	0.582±0.002	0.588±0.004	–0.002±0.011
Witten-Sander DLA	1.705±0.002	1.716±0.007	0.596±0.002	0.564±0.002	0.190±0.009

Results of the off-lattice DLA for 200 samples of N = 27,000 gives $\alpha = -0.002 \pm 0.011$ as shown in Fig. 8(Δ). Since its lattice is free from the special axis, size and length, a hottest tip irregularly grows on its direction or splits due to the effect of noise arising from the Monte Carlo method. On the other hand, a hottest tip of Witten-Sander DLA on square lattice has a finite angle of attack to hold its <10> growth even if the Brownian particle in outer field is simulated on off-lattice, which is obviously right angle. The existence of such an angle assures to maintain the growing direction of tip, and also this effect is enhanced by the coincidence with the direction of gradient of the field potential (Eckmann *et al.*, 1990). The hottest tip of off-lattice DLA has not hold any mechanisms to its growing direction. Therefore, such a tip growth can be recognized as a completely equalized type of frontal and lateral growths by the noise of field. Hence, homogeneous and self-similar DLA with the growth mechanism of random tip-splitting type appears as shown in Table 1.

Let us discuss the physical meaning of *kink-off* simulation. Supposing the Brownian particle is composed of a cluster of atoms, sputter-deposition (Elam *et al.*, 1985) and electrochemical deposition as shown in a transmission electro micrograph of zinc DLA by Grier *et al.* (1986) seem to be examples, all of effects

depending on the surface potential in *kink-on* simulation, i.e., surface nucleation, anisotropic hopping and kink effects become negligible. Such a particle, however, diffuses along the pattern surface until it loses kinetic energy. As a corresponding model, we can assume the conditions of $m = \gamma = 1$ and the lack of kink effect, and assume the surface random walk of τ steps for every adsorbed particle. This is our physical viewpoints on the *kink-off* simulations. Such a model is equivalent to the Witten-Sander DLA( ) model at $\tau = 0$, but according to the random walk of $\tau = 10$ steps along the pattern surface nearly isotropic pattern grows on the two-dimensional square lattice as shown in Fig. 8(+). The *kink-off* pattern of $\tau = 10$ yields $\alpha = 0.016 \pm 0.007$ for 300 samples of N = 128,000. Adsorbed particle arrived on the hottest tip randomly diffuses on the surface sites, and then grows at a site which is arbitrarily chosen among the unscreened and screened sites near the tip. Such a process derives to weaken the frontal growth and to strengthen the lateral growth. From this mechanism α shows smaller value than that of Witten-Sander DLA, and a nearly isotropic pattern is realized. However, it is assumed that the frontal growth occurs more frequently than the lateral one with the surface random walk of adsorbed particle in mind. Namely, the occupation probability of the particle after the surface random walk is greatest in the initial point arrived from the field. As a result of such effects, *kink-off* DLA yields very small <10> anisotropy as indicated in case of $\tau = 10$. However, <10> anisotropy decreases with increasing of τ, e.g., $\alpha = 0.003 \pm 0.012$ for 90 samples of $\tau = 100$ in N = 215,000. Fractal dimensions and characteristic exponents, however, indicate homogeneous and self-similar DLA as shown in Table 1 for *kink-off* DLA of $\tau = 10$. Although the dependence of τ in the *kink-off* DLA is an open problem, we can recognize it as nearly homogeneous and self-similar DLA within the error.

From these investigations for the growth mechanisms of the hottest tips in various kinds of aggregation model, it is indicated that the tip growth balanced between in the frontal and lateral surfaces can construct a homogeneous and self-similar DLA. And also, it is clarified that the random growth in the tip surface arising from the noise of field and arising from the random surface diffusion mechanisms enhances the homogeneity of patterns. And the tip growth with such a homogeneity mechanisms yields the randomly ramifying tip-splitting structure. Results for the various kinds of DLA are summarized in Table 1.

8. Homogeneous Dense-Radial-Like Aggregation

The importance of the random tip-splitting process to construct a homogeneous pattern can be indicated in the formation of a dense-radial-like pattern, which has been experimentally performed in the electrochemical deposition of zinc (Sawada *et al.*, 1986; Grier *et al.*, 1986, 1987). Dense-radial pattern grows radially from a cathode tip with the higher pattern density than DLA, and its global shape is holded circularity and homogeneity.

Result of the dense-radial-like pattern growing with the random tip-splitting

process is shown in Fig. 9, which is simulated on the square lattice for the pattern growth and on the off-lattice for the outer field. Excepting the drift motion of Brownian field particles towards the center (x = y = 0), this pattern is obtained from the same conditions as the crossover pattern of Fig. 3(d) in *kink-on* simulation, i.e., surface diffusion mechanism of $m = 5, \tau = 10$ and $\gamma = 0.23$. Here, the ratio of the flight length for the drift motion to that for the Brownian motion in the field sets equal to a quarter. This pattern is characterized by $\alpha = -0.02$, $\nu_{\parallel} \cong \nu_{\perp} \sim 0.52$ and $D \cong d_f \sim 1.93$. Such results clarify that the random tip-splitting growth constructs a homogeneous and self-similar aggregate irrespective of the drift motion in the outer field.

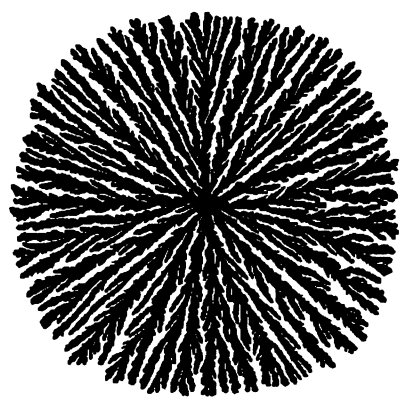

Fig. 9. Homogeneous and self-similar dense-radial-like pattern obtained from $m = 5$, $\tau = 10$, $\gamma = 0.23$, $r = 600$ and N = 680,000 under the drift motion of Brownian particles in the diffusion field.

Above pattern is simulated on square lattice with the kink effect, hence it corresponds to a single crystal in real pattern formation. Assuming the surface diffusion of cluster-like particle as indicated in *kink-off* DLA, and also assuming the polycrystaline lattice such as off-lattice DLA, constructing of completely circular dense-radial pattern as observed in zinc electrodeposit (Sawada *et al.*, 1986; Ben-Jacob *et al.*, 1986; Grier *et al.*, 1987) is anticipated.

9. Summary

In order to search for the relation between DLA and real pattern formation in especial dendritic crystal growth, new aggregation models including surface diffusion processes are performed on the two-dimensional square lattice by using the computer simulations not only under the boundary conditions of *kink-on* and *kink-off* cases in Laplace field but also under the drift motion in the diffusion field. Various kinds of the shapes closely related to the real crystal growth realize such

as <10> and <11> sidebranching dendritic patterns, hopper-like pattern, symmetric and asymmetric tip-splitting patterns, homogeneous and self-similar DLA patterns, and homogeneous dense-radial-like pattern.

From the results of *kink-on* simulation, the anisotropy whether pattern grows in <10> or <11> direction is classified by the growth mechanism of the hottest tips whether it is frontal or lateral type. According to a new measure of pattern anisotropy α, the ramifying morphology can be grouped into two classes of sidebranching phase in $|\alpha| \geq 0.5$ and of tip-splitting phase in $|\alpha| \leq 0.5$. The tip growth of random tip-splitting type in the anisotropy crossover domain of $\alpha \sim 0$ constructs a homogeneous and self-similar DLA with the fractal dimension of $d_f \cong 1.716$ under the existence of the adequate noise. Such a tip growth produces a homogeneous and self-similar dense-radial-like pattern under the drift motion in the outer diffusion field. Therefore, we can conclude that the homogeneous and self-similar on-lattice patterns come into existence in the anisotropy crossover domain due to the anisotropy reducing effects by noise.

Such considerations on the close relation between the growth mechanism of the hottest tips and the anisotropy of pattern are not only valid for the anisotropies of Witten-Sander DLA and nearly homogeneous *kink-off* DLA but also valid for the homogeneity of off-lattice DLA.

Fractal dimension $d_f \cong 1.716$ of homogeneous DLA obtained from the radius-of-gyration exponent and $D \cong 1.715$ obtained from the finite-scaling analysis are consistent each other and also consistent with $d_f = 1.715$ of off-lattice DLA. However, these values are inconsistent with the theoretical value of $d_f = 5/3$ (Muthukumar, 1983; Tokuyama and Kawasaki, 1984; Honda *et al.*, 1986). Such a theoretical value agrees with the fractal dimension of the anisotropy coexistent pattern rather than that of DLA. Turkevich and Scher (1985) and Ball *et al.* (1985b) have discussed the fractal dimension of DLA from a standpoint of the growth probability in the hottest tips. Present results point out that the balancing mechanism between unscreened and screened surfaces in the hottest tips needs to construct the homogeneous and self-similar pattern. Accordingly, it is an interesting problem whether new theoretical approach to the fractal dimension of DLA based on present considerations is possible or not.

The *kink-on* simulations yield various kinds of crystal-like patterns such as regular, hopper, needle, sidebranching, tip-stable and tip-splitting patterns. These results not only indicate that the boundary conditions of anisotropy and noise are essentially important for the dendritic pattern formation, but also indicate that the present model is closely related to the real dendritic crystal growth. However, some of the assumptions, e.g., constant values of m and τ and also ignorance of the evaporation process from the pattern, have been used for the simplicities of the discussions and of the simulations. Therefore, correspondences between the present parameters and the realistic nonequilibrium parameter of supercooling or supersaturation are not clear. Nevertheless, noise effect, anisotropy through the hopping mechanism of surface diffusion particles and anisotropy of surface tension

originated in surface kinetics are realized. Present results must play an important role in the analysis and discussions of the complicated ramifying structures growing in the nonlinear and nonequilibrium systems.

Finally, we can deduce the following classification on the pattern formation growing in the diffusion fields. The DLA pattern is generated in the homogeneous Laplace systems carried with sufficient amount of fluctuation, e.g., viscous fingering in the miscible liquids (Wong, 1988), electrodeposition constituted by cluster (Grier *et al.*, 1986) and crystal growth in the randomness imposed cell (Honjo *et al.*, 1986). The additional boundary condition of isotropic surface tension turns system into the problem of Hele Shaw cell. The addition of anisotropic boundary conditions makes DLA system change into the crystal growth. And the inclusion of drift motion in the diffusion field, i.e., the decrease of the diffusion length induces the dense-radial growth. Diversity of real dendritic pattern formation comes into existence from the competition of those conditions.

Acknowledgements

I would like to thank M. Matsushita and K. Honda for many useful comments and discussions during the preliminary stage of this work. I am particularly grateful to H. Honjo for giving me some advices and suggestions from the experimental viewpoint of dendritic crystal growth. I would also like to thank Y. Sawada who has indicated me closed connection with real pattern formations. I acknowledge useful conversations with P. Meakin, A. Libchaber, J. S. Langer, K. Kawasaki, T. Kuroda, Y. Saito, M. Uwaha and H. Mori. I wish to thank T. Kawabe for the computer treatment. This work was partially supported by the Takeda Science Foundation.

REFERENCES

Ball, R. C. and Brady, R. M. (1985a), Large scale lattice effect in diffusion-limited aggregation, J. Phys. A, **18**, L809–L813.

Ball, R. C., Brady, R. M., Rossi, G., and Thompson, B. R. (1985b), Anisotropy and cluster growth by diffusion-limited aggregation, Phys. Rev. Lett., **55**, 1406–1409.

Barbieri, A., Hong, D. C., and Langer, J. S. (1987), Velocity selection in the symmetric model of dendritic crystal growth, Phys. Rev. A, **35**, 1802–1808.

Bechhoefer, J. and Libchaber, A. (1987), Testing shape selection in directional solidification, Phys. Rev. B, **35**, 1393–1396.

Ben-Jacob, E., Godby, R., Goldenfeld, N. D., Koplik, J., Levin, H., Muller, T., and Sander, L. M. (1985), Experimental demonstration of the role of anisotropy in interfacial pattern formation, Phys. Rev. Lett., **55**, 1315–1318.

Bensimon, D., Kadanoff, L. P., Liang, S., Shraiman, B. I., and Tang, C. (1986), Viscous flows in two dimensions, Rev. Mod. Phys., **58**, 977–999.

Brower, R. C., Kessler, D. A., Koplik, J., and Levine, H. (1983), Geometrical approach to moving-interface dynamics, Phys. Rev. Lett., **51**, 1111–1114.

Chan, S.-K., Reimer, H.-H., and Kahlweit, M. (1976), On the stationary growth shapes of NH_4Cl dendrites, J. Crystal Growth, **32**, 303–315.

Daccord, G., Nittmann, J., and Stanley, H. E. (1986), Radial viscous fingers and diffusion-limited

aggregation: fractal dimension and growth sites, Phys. Rev. Lett., **56**, 336–339.
Dougherty, A., Kaplan, P. D., and Gollub, J. P. (1987), Development of side branching in dendritic crystal growth, Phys. Rev. Lett., **58**, 1652–1655.
Eckmann, J.-P., Meakin, P., Procaccia, I., and Zeitak, R. (1989), Growth and form of noise-reduced diffusion-limited aggregation, Phys. Rev. A, **39**, 3185–3195.
Eckmann, J.-P., Meakin, P., Procaccia, I., and Zeitak, R. (1990), Asymptotic shape of diffusion-limited aggregates with anisotropy, Phys. Rev. Lett., **65**, 52–55.
Elam, W. T., Wolf, S. A., Sprague, J., Gubser, D. U., Van Vechten, D., Barz, G. L., Jr., and Meakin, P. (1985), Fractal aggregates in sputter-deposited $NbGe_2$ films, Phys. Rev. Lett., **54**, 701–703.
Family, F. and Landau, D. P. (1984), Kinetics of aggregation and gelation, North-Holland, Amsterdam.
Grier, D., Ben-Jacob, E., Clarke, R., and Sander, L. M. (1986), Morphology and microstructure in electrochemical deposition of zinc, Phys. Rev. Lett., **56**, 1264–1267.
Grier, D. G., Kessler, D. A., and Sander, L. M. (1987), Stability of the dense radial morphology in diffusive pattern formation, Phys. Rev. Lett., **59**, 2315–2318.
Harsey, T. C., Jensen, M. H., Kadanoff, L. P., Procaccia, I., and Shraiman, B. I. (1986), Fractal measures and their singularities: the characterization of strange sets, Phys. Rev. A, **33**, 1141–1151.
Hayakawa, Y., Sato, S., and Matsushita, M. (1987), Scaling structure of the growth-probability distribution in diffusion-limited aggregation processes, Phys. Rev. A, **36**, 1963–1966.
Honda, K., Toyoki, H., and Matsushita, M. (1986), A theory of fractal dimensionality for generalized diffusion-limited aggregation, J. Phys. Soc. Jpn., **55**, 707–710.
Honjo, H., Ohta, S., and Sawada, Y. (1985), New experimental findings in two-dimensional dendritic crystal growth, Phys. Rev. Lett., **55**, 841–844.
Honjo, H., Ohta, S., and Matsushita, M. (1986), Irregular fractal-like crystal growth of ammonium chloride, J. Phys. Soc. Jpn., **55**, 2487–2490.
Honjo, H., Ohta, S., and Matsushita, M. (1987), Phase diagram of a growing succinonitrille crystal in supercooling-anisotropy phase space, Phys. Rev. A, **36**, 4555–4558.
Huang, S.-C. and Glicksman, M. E. (1981), Fundamentals of dendritic solidification I. Steady-state tip growth, Acta Metall., **29**, 701–715.
Huang, S.-C. and Glicksman, M. E. (1981), Fundamentals of dendritic solidification II. Development of sidebranch structure, Acta Metall., **29**, 717–734.
Ivantsov, G. P. (1947), Temperature field around a spherical, cylindrical and acicular crystal growing in a supercooled melt, Dokl. Akad. Nauk SSSR, **58**, 567–569.
Kertész, J. and Vicsek, T. (1986), Diffusion-limited aggregation and regular patterns: fluctuations versus anisotropy, J. Phys. A, **19**, L257–L262.
Kessler, D. A., Koplik, J., and Levine, H. (1985), Geometric models of interface evolution. III. Theory of dendritic growth, Phys. Rev. A, **31**, 1712–1717.
Langer, J. S. and Muller-Krumbhhar (1978), Theory of dendritic growth I. Elements of a stability analysis, Acta Metall., **26**, 1681–1687.
Langer, J. S. and Muller-Krumbhhar (1978), Theory of dendritic growth II. Instabilities in the limit of vanishing surface tension, Acta Metall., **26**, 1689–1695.
Langer, J. S. and Muller-Krumbhhar (1978), Theory of dendritic growth III. Effects of surface tension, Acta Metall., **26**, 1697–1708.
Langer, J. S. (1980), Instabilities and pattern formation in crystal growth, Rev. Mod. Phys., **52**, 1–28.
Langer, J. S. (1986), Existence of needle crystals in local models of solidification, Phys. Rev. A, **33**, 435–441.
Langer, J. S. (1989), Dendrites, viscous fingers, and the theory of pattern formation, Science, **243**, 1150–1156.
Liang, S. (1986), Random-walk simulations of flow in Hele Shaw cells, Phys. Rev. A, **33**, 2663–2674.
Liu, F. and Goldenfeld, N. (1988), Linear stability of needle crystals in the boundary-layer model of dendritic solidification, Phys. Rev. A, **38**, 407–417.
Mandelbrot, B. B. (1977), Fractals, Form, Chance, and Dimension, Freeman, San Francisco, pp. 58–59.

Mandelbrot, B. B. (1982), The fractal geometry of nature, Freeman, San Francisco, pp. 349–350.
Matsushita, M., Sano, M., Hayakawa, Y., Honjo, H., and Sawada, Y. (1984), Fractal structures of zinc metal leaves growth by electrodeposition, Phys. Rev. Lett., **53**, 286–289.
Matsushita, M. and Kondo, H. (1986), Diffusion-limited aggregation with tunable lattice anisotropy, J. Phys. Soc. Jpn., **55**, 2483–2486.
Matsushita, M., Hayakawa, Y., Sato, S., and Honda, K. (1987), Scaling properties for the unscreened surfaces of fractal patterns, Phys. Rev. Lett., **59**, 86–89.
Meakin, P. and Sander, L. M. (1985), Comment on "active zone of growing clusters: diffusion-limited aggregation and the Eden model", Phys. Rev. Lett., **54**, 2053.
Meakin, P. (1986a), Computer simulation of growth and aggregation processes, in On growth and form, edited by Stanly, H. E. and Ostrowsky, N., Martinus Nijhoff, the Hague, pp. 119–126.
Meakin, P. and Family, F. (1986b), Diverging length scales in diffusion-limited aggregation, Phys. Rev. A, **34**, 2558–2560.
Meakin, P., Ball, R. C., Ramanlal, P., and Sander, L. M. (1987), Structure of large two-dimensional square-lattice diffusion-limited aggregates: approach to asymptotic behavior, Phys. Rev. A, **35**, 5233–5239.
Miller, A., Knoll, W., and Mohwald, H. (1986), Fractal growth of crystallin phospholipid domains in monolecular layers, Phys. Rev. Lett., **56**, 2633–2636.
Mullins, W. W. and Sekerka, R. F. (1964), Stability of a planar interface during solidification of a dilute binary alloy, J. Appl. Phys., **35**, 444–451.
Muthukumar, M. (1983), Mean-field theory for diffusion-limited cluster formation, Phys. Rev. Lett., **50**, 839–842.
Niemeyer, L., Pietronero, L., and Wiesmann, H. J. (1984), Fractal dimension of dielectric breakdown, Phys. Rev. Lett., **52**, 1033–1036.
Nittmann, J. and Stanley, H. E. (1986), Tip splitting without interfacial tension and dendritic growth patterns arising from molecular anisotropy, Nature, **321**, 663–668.
Ohta, S. and Honjo, H. (1988), Growth probability distribution in irregular fractal-like crystal growth of ammonium chloride, Phys. Rev. Lett., **60**, 611–614.
Pelcé, P. (1988), Dynamics of curved fronts, Academic Press, London.
Paterson, L. (1985), Fingering with miscible fluids in a Hele Shaw cell, Phys. Fluids, **28**, 26–30.
Pieters, R. and Langer, J. S. (1986), Noise-driven sidebranching in the boundary-layer model of dendritic solidification, Phys. Rev. Lett., **56**, 1948–1951.
Pietronero, L. and Tosatti, E. (1985), Fractals in Physics, North-Holland, Amsterdam.
Saffman, P. G. and Taylor, G. I. (1958), The penetration of a fluid into a porous medium or Hele-Shaw cell containing a more viscous liquid, Proc. Roy. Soc. A, **245**, 312–329.
Sawada, Y., Dougherty, A., and Gollub, J. P. (1986), Dendri and fractal patterns in electrolytic metal deposits, Phys. Rev. Lett., **56**, 1260–1263.
Stanley, H. E. and Ostrowsky, N. (1985), On growth and form, Martinus Nijhoff, the Hague.
Tang, C. (1985), Diffusion-limited aggregation and the Saffman-Taylor problem, Phys. Rev. A, **31**, 1977–1979.
Tao, R., Novotny, M. A., and Ksaki, K. (1988), Diffusion-limited aggregation with surface tension, Phys. Rev. A, **38**, 1019–1026.
Tokuyama, M. and Kawasaki, K. (1984), Fractal dimensions for diffusion-limited aggregation, Phys. Lett., **100A**, 337–340.
Turkevich, L. A. and Scher, H. (1985), Occupancy-probability scaling in diffusion-limited aggregation, Phys. Rev. Lett., **55**, 1026–1029.
Vicsek, T. (1984), Pattern formation in diffusion-limited aggregation, Phys. Rev. Lett., **53**, 2281–2284.
Vicsek, T. (1985), Formation of solidification patterns in aggregation models, Phys. Rev. A, **32**, 3084–3089.
Vicsek, T. (1989), Fractal growth phenomena, World Scientific, Singapore.
Witten, A and Sander, L. M. (1981), Diffusion-limited aggregation, a kinetic critical phenomenon, Phys.

Rev. Lett., **47**, 1400–1403.
Wong, P.-Z. (1988), The statistical physics of sedimentary rock, Phys. Today, **41**, 24–32.
Xiao, R., Alexander, J. I. D., and Rosenberger, F. (1988), Morphological evolution of growing crystals: A Monte Carlo simulation, Phys. Rev. A, **38**, 2447–2456.